

Natural climate variability and teleconnections to precipitation over the Pacific-North American region in CMIP3 and CMIP5 models

Suraj D. Polade,¹ Alexander Gershunov,¹ Daniel R. Cayan,^{1,2} Michael D. Dettinger,² and David W. Pierce¹

Received 25 February 2013; revised 16 April 2013; accepted 18 April 2013.

[1] Natural climate variability will continue to be an important aspect of future regional climate even in the midst of long-term secular changes. Consequently, the ability of climate models to simulate major natural modes of variability and their teleconnections provides important context for the interpretation and use of climate change projections. Comparisons reported here indicate that the CMIP5 generation of global climate models shows significant improvements in simulations of key Pacific climate mode and their teleconnections to North America compared to earlier CMIP3 simulations. The performance of 14 models with simulations in both the CMIP3 and CMIP5 archives are assessed using singular value decomposition analysis of simulated and observed winter Pacific sea surface temperatures (SSTs) and concurrent precipitation over the contiguous United States and northwestern Mexico. Most of the models reproduce basic features of the key natural mode and their teleconnections, albeit with notable regional deviations from observations in both SST and precipitation. Increasing horizontal resolution in the CMIP5 simulations is an important, but not a necessary, factor in the improvement from CMIP3 to CMIP5. **Citation:** Polade, S. D., A. Gershunov, D. R. Cayan, M. D. Dettinger, and D. W. Pierce (2013), Natural climate variability and teleconnections to precipitation over the Pacific-North American region in CMIP3 and CMIP5 models, *Geophys. Res. Lett.*, 40, doi:10.1002/grl.50491.

1. Introduction

[2] Large-scale climate variability in the Pacific region significantly influences the regional hydroclimate of North America. The El Niño–Southern Oscillation (ENSO) and Pacific Decadal Oscillation (PDO) [Mantua *et al.*, 1997] are the dominant natural modes of climate variability over the Pacific region and influence North American precipitation through their impact on atmospheric circulation [e.g., Gershunov and

Barnett, 1998a, 1998b; Hu and Feng, 2012]. Several studies show that a constructive combination of El Niño and the warm phase of the PDO favors precipitation over southwest North America and drying in the Ohio River Valley, with the reverse during La Niña and the cold phase of the PDO [Gershunov and Barnett, 1998b; McCabe and Dettinger, 1999].

[3] There is also evidence that the ENSO and the PDO influence extreme events over North America. For example, Swetnam and Betancourt [1998] and Cook *et al.* [1999] showed the influence of ENSO on U.S. drought. Similarly, Westerling and Swetnam [2003] showed the influence of PDO on drought. These large-scale modes of Pacific variability exhibit strongest teleconnections in winter [Gershunov and Cayan, 2003]. Beyond the mean winter climate, both together and separately, they influence the frequency of extreme daily temperature and heavy precipitation as well as streamflow [Gershunov and Barnett, 1998a, 1998b; Cayan *et al.*, 1999; Gershunov and Cayan, 2003].

[4] Realistic modeling of climate change impacts on regional precipitation patterns requires that general circulation models (GCMs) realistically represent ENSO and its teleconnections [Douville *et al.*, 2006]. Recently, attention has been focused on the realism of CMIP5 models [Taylor *et al.*, 2012] compared to the older-generation CMIP3 models [Meehl *et al.*, 2000]. Climate modeling centers have compared representations of mean climate states, precipitation patterns, ENSO variability, and large-scale circulation in CMIP3- and CMIP5-generation individual models [Rotstayn *et al.*, 2010; Donner *et al.*, 2011]. Most recently, comparisons began between the ensemble performance of CMIP3 and CMIP5 models [Kug *et al.*, 2012]. Most investigators have noted the improvement in CMIP5 models in representing these climatic aspects compared to CMIP3 models. Recent studies by Langenbrunner and Neelin [2013] and Zhang *et al.* [2012] investigated the model fidelity by means of ENSO teleconnections to precipitation. In this study, we diagnose the structure of teleconnections between Pacific climate variability and the regional hydroclimate of North America, assess the performance of fourteen CMIP5 models compared to their CMIP3 counterparts in their ability to simulate the observed teleconnected structure, and discuss factors responsible for the improvements found. Specifically, we diagnose coupled modes of variability in (a) winter precipitation accumulations over a broad swath of North America (contiguous United States and northwest Mexico) and (b) sea surface temperature (SST) over the tropical and North Pacific Ocean. In our analysis, ENSO and PDO are revealed and summarized in a single mode of teleconnected variability (see section 4). We know that ENSO and PDO are not distinct

Additional supporting information may be found in the online version of this article.

¹Climate, Atmospheric Science and Physical Oceanography (CASPO), Scripps Institution of Oceanography, La Jolla, California, USA.

²United States Geologic Survey, La Jolla, California, USA.

Corresponding author: S. D. Polade, Climate, Atmospheric Science and Physical Oceanography, Scripps Institution of Oceanography, 9500 Gilman Dr. La, Jolla, CA 92093, USA. (spolade@ucsd.edu)

©2013. American Geophysical Union. All Rights Reserved.
0094-8276/13/10.1002/grl.50491

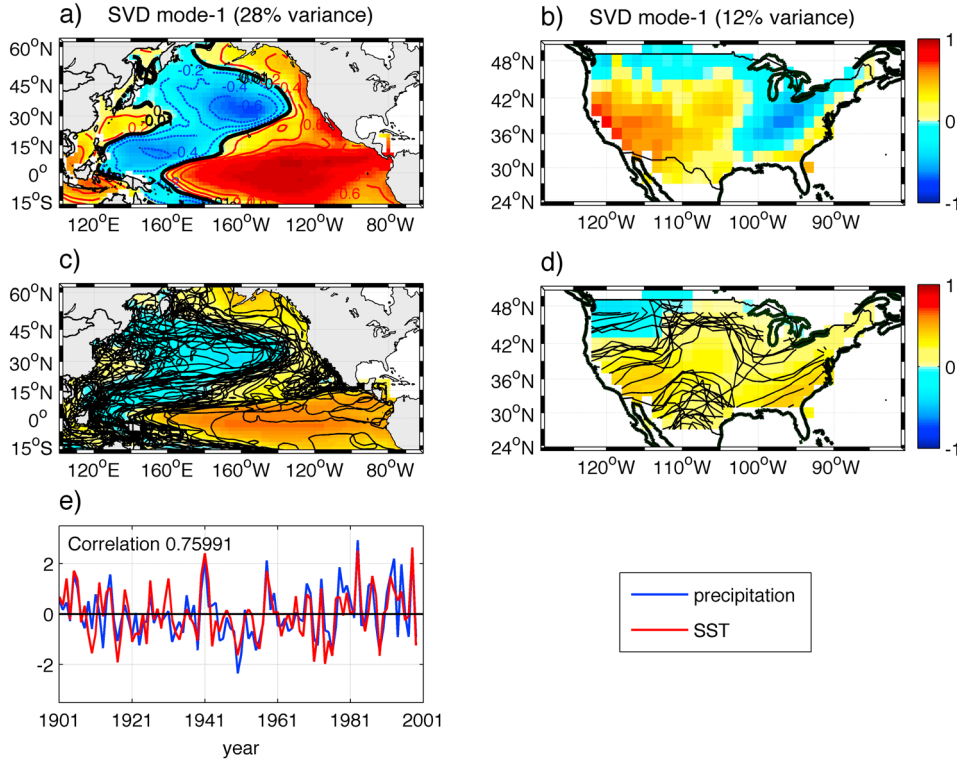


Figure 1. Observed loading patterns of first SVD mode for (a) SST and (b) precipitation, and SVD time series, for (e) winter (in normalized values). Average leading SVD loading patterns for all the models for (Figure 1c) SST and (Figure 1d) precipitation. The SVD loading patterns are expressed as a correlation between SVD time series and respective variables. (e) Red and blue lines denote SST and precipitation, respectively. Black lines in Figures 1c and 1d indicate zero contour lines for individual models.

from one another [Schneider and Cornuelle, 2005] and neither are their impacts on North American hydroclimate [Gershunov and Barnett, 1998b], so their constructive interaction is naturally summarized in one linear mode as in Gershunov and Cayan [2003] (see section 4 and Figure S2 for details). Besides providing feedback to the modeling community, the results may serve as a useful metric for model selection in the studies of regional climate projections.

2. Model Output and Observational Data

[5] We analyze the historical simulations of 14 climate models with versions that participated in both the CMIP3 and CMIP5 experiments. The historical simulations were forced with natural solar and volcanic variations and anthropogenic radiative forcings, extending from 1850 to 1999 in CMIP3 and to 2005 in CMIP5. The 14 CMIP3 and CMIP5 model pairs are listed in the supplementary online material (Table S1). Monthly Pacific SST and precipitation over North America were analyzed and compared with observations over the period 1901–1999.

[6] Monthly observed precipitation over the contiguous United States and northwest Mexico gridded at 1° spatial resolution are from the Global Precipitation Climatology Centre-V5 rainfall analyses [Schneider et al., 2011]. Monthly average SST observations are from the Extended Reconstructed Sea Surface Temperature v3b [Smith et al., 2008] data set. SST and precipitation observations are available until near present, starting from 1854 and 1901, respectively. We consider January–February–March (JFM) SST

and precipitation since it is the season with strongest teleconnections [e.g., Gershunov and Cayan, 2003]. For a fair comparison, both modeled and observed SST and precipitation fields were remapped to a regular $2^\circ \times 2^\circ$ grid by using bilinear interpolation.

3. Methodology

[7] The teleconnections were assessed by singular value decomposition (SVD) of the cross-covariance matrix between detrended SST over the Pacific Ocean (north of 30°S) and North American precipitation. Before performing the SVD analysis, a linear trend was removed from all individual grid point time series. We limited our analysis by focusing mainly on the first SVD mode, since the first mode usually captures the ENSO-PDO pattern and much of the teleconnection to precipitation. However, for certain models (five models from CMIP3 and three models from CMIP5), the second SVD mode was considered when it captured an ENSO-PDO spatial pattern. Details of the methodology can be found in the online supporting information.

4. Observed Teleconnections

[8] The first SVD mode of observed JFM-averaged SST and precipitation (Pr) (Figure 1a) captures a combination of ENSO and PDO variability (see Figure S2 for details). Two regions of highest loading with opposite sign are also observed in precipitation: one over the southwest United States and another over the Ohio River Valley (Figure 1b). This SVD

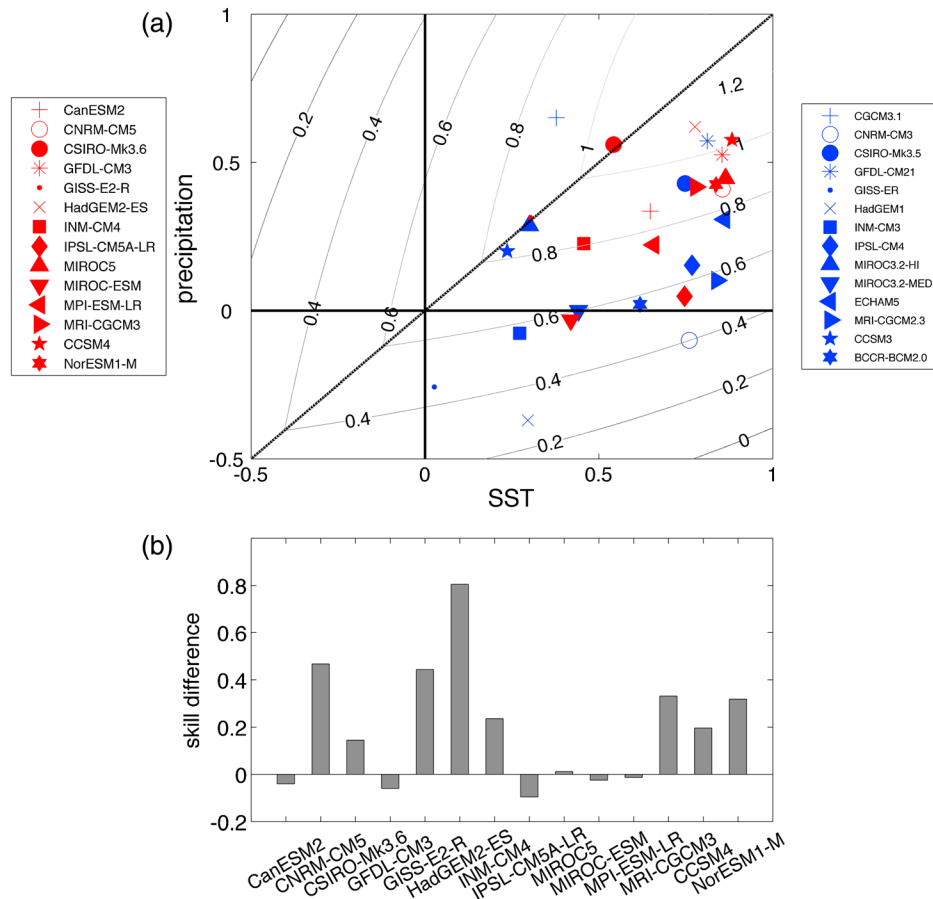


Figure 2. (a) Pattern correlation of the leading SVD mode of modeled and observed SST *versus* pattern correlation of the leading SVD mode of modeled and observed precipitation. Blue and red symbols represent CMIP3 and CMIP5 models, respectively. Grey contour lines indicate model skill (higher values mean greater skill; see text for details). (b) The skill difference between CMIP5 and CMIP3 models (see text for details).

mode explains the combined ENSO and PDO large-scale variability and their teleconnections with hydroclimate of North America in a single pair of map [Gershunov and Cayan, 2003]. The leading mode explains 28% and 12% of the variability in detrended Pacific SST and North American precipitation, respectively. Regionally, however, up to 90% of the SST variance in the central tropical Pacific and 55% in the central North Pacific, as well as up to 73% of precipitation variance in the southwestern United States, are captured by this leading mode.

[9] The strength of the association between the two fields is measured by the percentage explained squared covariance by the spatial patterns of the first SVD mode and the temporal correlation coefficient between SVD time series of SST (TS_{SST}) and Pr (TS_P). The Pacific SST field is strongly linked with North American precipitation, which explains 79% of total squared covariance. The temporal correlation between the SVD time series is 0.76, which is significant at 98% confidence level by t statistics. The correlation between TS_{SST} and Nino3.4 index (average SST over Nino3.4 region; $170^{\circ}W-120^{\circ}W$ $5^{\circ}S-5^{\circ}N$) is 0.94, implying strong links between regional precipitation and ENSO. Strong El Niño (1905, 1930, 1941, 1957, 1965, 1972, 1982, and 1997) and La Niña (1910, 1916, 1945, 1973, 1975, 1988, and 1999) events are prominent in the SVD time series (Figure 1e). Both El Niño and La Niña events are stronger and more frequent

during 1950–1999 compared to the earlier half century. The SVD time series also shows a major shift in the late 1970s, consistent with the decadal phase shift in PDO [Graham 1994; Mantua *et al.*, 1997]. The leading SVD mode represents the constructive interaction of ENSO and PDO teleconnections discussed by Gershunov and Barnett [1998b], which promotes stronger ENSO teleconnections to North American precipitation.

5. Modeled Teleconnections

[10] The ensemble-average SVD loading patterns (Figure 1c) from the 28 models (14 models pairs) are quite similar to that of the observed patterns for SST. While for precipitation, on average, models have good agreement with observation over southwest United States (Figure 1d) but failed to capture the observed SVD pattern over the Ohio River Valley. However, individual models vary in how well they reproduce the observed precipitation pattern in specific regions. For example, CanESM2*, CGCM3.1#, CSIRO-Mk3-6-0*, CSIRO-Mk3.5#, GISS-E2-R*, MIROC5*, MPI-ESM-LR*, and CCSM4* best represent the observed teleconnections over southwest United States, while CNRM-CM5*, GFDL-CM21#, HadGEM2-ES*, and MIROC3.2-HI# best represent the observed teleconnections over Ohio River Valley (* denotes CMIP5 model; # denotes CMIP3 model). In the ensemble average, models underestimate

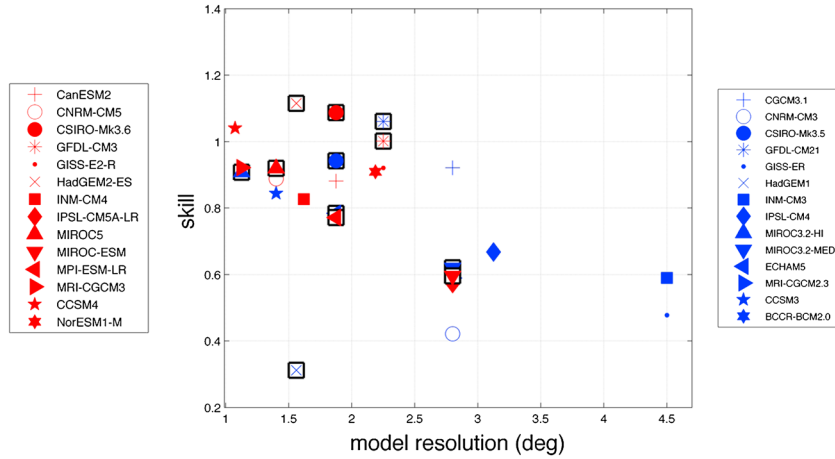


Figure 3. The models’ skill with respect to horizontal resolution. Blue and red symbols represent CMIP3 and CMIP5 models, respectively, while black squares indicate the models that did not improve horizontal resolution from CMIP3 to CMIP5. A perfect model would have skill of $\sqrt{2}$.

the observed SST and precipitation SVD loading, while individual models can underestimate or overestimate it. The solid black lines in Figures 1c and 1d are the zero contour lines for individual models. However, the large discrepancies in the zero contour lines emphasize that individual models can strongly differ from the ensemble mean. In general, models agree with observations more in the tropics than in the North Pacific (Figure S2). The percentage explained squared covariance captured by the first SVD mode ranges from 17% to 87% for CMIP3 models with temporal correlation of 0.47–0.73 between their SVD time series, while for CMIP5 models, percentage explained squared covariance ranges from 19% to 90% with temporal correlation of 0.34–0.69. The temporal correlations shown here are significant at 98% confidence level by *t* statistics for all the models. The percentage explained squared covariance and temporal correlation in SVD time series are generally smaller than those in observations for most of the models, while CMIP3 and CMIP5 models do not significantly differ from each other in this respect.

[11] Since the correlation between TS_{SST} and TS_P is a measure of how two fields of variables covary, the individual models can have a realistic correlation even if they do not realistically capture the observed SVD patterns. Therefore, we quantify model skill in representing large-scale climate variability and its teleconnections by spatial correlations between modeled and observed SVD patterns of SST and precipitation. Figure 2a displays SST versus precipitation pattern correlations with the observations for each of the 28 models. A model that perfectly reproduced the observed patterns would be positioned at (1,1). CMIP5 models are closer to the (1,1) point compared to CMIP3 models, showing a tendency to perform better than CMIP3 models. Most of the models represent SST patterns better than precipitation. In general, models show tendencies to underestimate the strongest observed ENSO (tropical) and the PDO (North Pacific) loading; however, CMIP5 models show smaller deviations from the observations over both regions compared to CMIP3 models (Figures S1 and S2 in supplementary material).

[12] Each model’s skill is taken as the mean of two distances: from the model’s point in Figure 2a to the perfect

skill point (1,1) and to the diagonal. The distance from the diagonal is considered in the skill measure in order to represent equal contribution of both SST and precipitation patterns, as representation of both patterns is of equal importance for the teleconnection. The nondimensional result reflects both how close to perfectly reproducing the observations the model is and how equally the model captures the SST and precipitation patterns; models that do very well in one pattern but poorly in the other are penalized. The resulting metric has lower values for better models, so for convenience, we subtract this number from $\sqrt{2}$ [the distance from the origin to the perfect point (1,1)], yielding a final skill value that increases as model skill increases (Figure 2a, contours). Nine of the 14 CMIP5 models show improvement with respect to the paired CMIP3 models (averaging 0.33; Figure 2b), while the other five models show marginal degradation (averaging -0.05).

6. Causes of Improved CMIP5 Performance

[13] In order to understand the reasons why ENSO and PDO variability and their teleconnections were generally better represented in CMIP5 models than in CMIP3 models, we first examined the relationship between the models’ skill and the horizontal resolution (Figure 3). In general, finer resolution models have better skill than coarser resolution models. This result demonstrates that resolution is one of the important factors determining models’ skills.

[14] Most models in which horizontal resolution increased from CMIP3 to CMIP5 yield strong improvements in skill with increasing resolution, except CAN-ESM2 and IPSL-CM5A-LR. However, the HadGEM2-ES model shows a large improvement with respect to its previous generation CMIP3 counterpart without improvement in resolution, demonstrating that other factors, such as changes in model physics and/or aerosol forcing, can significantly contribute to better model skill. Consequently, the effect of improved model physics and aerosol forcing on model skill was also assessed, as CMIP5 models often included more sophisticated model physics and aerosol treatments. Most of the modeling centers either replaced the existing physical parameterization schemes with more sophisticated parameterizations or else improved

the existing parameterizations significantly, except for INM-CM4 model, from CMIP3 to CMIP5, details of which can be found in online supporting information (Table S2). Since several of the models that improved resolution also changed model physics, it is difficult to separate out the contribution of these individual factors in improving skill. The large improvement in HadGEM2-ES model skill of 0.81 (Figure 2b) is mostly due to changes in model physics, as there is no change in resolution, whereas the 0.25 skill improvement observed for INM-CM4 compared to its CMIP3 version is mostly due to an improvement in model resolution. The GFDL-CM3 model's performance degrades (although not significantly) even after significant changes in model physics. No clear dependency of models' skill on inclusion of more aerosol species, volcanic aerosols, or aerosol indirect effects was found.

7. Concluding Remarks

[15] We have examined the representation of the leading natural mode of teleconnected Pacific SST variability to North American winter precipitation in 28 simulations of historical climate, using 14 model pairs that have versions in both the CMIP3 and CMIP5 archives. Using SVD analysis, modeled teleconnections were evaluated and compared to those observed. To understand the effect of model changes, we then compared the representation of these teleconnections in the CMIP5 version of the GCMs to the CMIP3 version for each of the 14 pairs. In observations, the leading SVD mode is a combined ENSO and PDO SST mode with strong teleconnections to North American winter precipitation [e.g., *Gershunov and Barnett*, 1998b]. Overall, most models reproduced the basic features of the natural mode and their teleconnections, albeit with notable regional deviations from reality in both SST and precipitation. CMIP5 versions show clear improvement in nine of the 14 models compared to the corresponding CMIP3 versions. Improved model resolution and physics are the most important factors responsible for these improvements, but it is difficult to separate the relative contributions of these factors since models typically evolved both. We found examples where model skill improved only due to increased resolution (INM-CM4), as well as only due to improved physics (HadGEM2-ES). This supports both *Gualdi et al.* [2005], who noted improvement in ENSO and precipitation characteristics with increasing resolutions, and *Mo et al.* [2005], who noted improvement in precipitation characteristics with improved model physics. There is no clear dependency of models' skill improvement on the inclusion of more aerosol species or improved aerosol forcing. However, because sample sizes are small and model developments vary from GCM to GCM, the individual contributions from improved model physics and resolutions cannot be identified reliably here.

[16] Although the ensemble of model simulations captures the structure of the observed teleconnected signal reasonably well, especially for CMIP5 models, model intercomparison presented here is helpful in choosing the best models for regional applications, such as in the southwest United States or the Ohio River Valley. A reasonable next step would be to look at how these projected teleconnections are to be affected by climate change, as PDO can result in apparent

trends in records spanning decades and interfere with the anthropogenic signal.

[17] **Acknowledgments.** This work was supported by DOI via the Southwest Climate Science Center and by NOAA via the RISA program through the California and Nevada Applications Center, and by the California Energy Commission PIER Program via the California Climate Change Center at the Scripps Institution of Oceanography. We thank Mary Tyree for archiving CMIP3 and CMIP5 data sets and making them available locally.

[18] The Editor thanks two anonymous reviewers for their assistance in evaluating this paper.

References

- Cayan, D. R., K. T. Redmond, and L. G. Riddle (1999), ENSO and hydrologic extremes in the western United States, *J. Clim.*, *12*, 2881–2893.
- Cook, E. R., J. E. Cole, R. D. D'Arrigo, D. W. Stahle, and R. Villalba (1999), Tree ring records of past ENSO variability and forcing, in *El Niño and the Southern Oscillation: Multiscale Variability and its Impacts on Natural Ecosystems and Society*, edited by H. F. Diaz and V. Markgraf, Cambridge Univ. Press, Cambridge, U.K. in press.
- Donner, L. J., B. L. Wyman, R. S. Hemler, L. W. Horowitz, Y. Ming, M. Zhao, J.-C. Golaz, et al. (2011), The dynamical core, physical parameterizations, and basic simulation characteristics of the atmospheric component AM3 of the GFDL global coupled model CM3, *J. Clim.*, *24*(13), 3484–3519, doi:10.1175/2011JCLI3955.1.
- Douville, H., D. Salas-Méla, and S. Tyteca (2006), On the tropical origin of uncertainties in the global land precipitation response to global warming, *Clim. Dyn.*, *26*, 367–385.
- Gershunov, A., and T. Barnett (1998a), ENSO influence on intraseasonal extreme rainfall and temperature frequencies in the contiguous US: Observations and model results, *J. Clim.*, *11*, 1575–1586.
- Gershunov, A., and T. Barnett (1998b), Interdecadal modulation of ENSO teleconnections, *Bull. Am. Meteorol. Soc.*, *79*, 2715–2725.
- Gershunov, A., and D. Cayan (2003), Heavy daily precipitation frequency over the contiguous United States: Sources of climate variability and seasonal predictability, *J. Clim.*, *16*, 2752–2765, doi:10.1175/1520-0442(2003)016<2752:HDPFOT>2.0.CO;2.
- Graham, N. E. (1994), Decadal-scale climate variability in the tropical and North Pacific during the 1970s and 1980s—Observations and model results, *Clim. Dyn.*, *10*, 135–162.
- Gualdi, S., A. Alessandri, and A. Navarra (2005), Impact of atmospheric horizontal resolution on El Niño Southern Oscillation forecasts, *Tellus, Ser. A*, *57*(A), 357–374.
- Hu, Q., and S. Feng (2012), AMO and ENSO driven summertime circulation and precipitation variations in North America, *J. Clim.*, *25*, 6477–6495, doi:10.1175/JCLI-D-11-00520.1.
- Kug, J.-S., Y.-G. Ham, J.-Y. Lee, and F.-F. Jin (2012), Corrigendum: Improved simulation of two types of El Niño in CMIP5 models, *Environ. Res. Lett.*, *7*(3), 039502, doi:10.1088/1748-9326/7/3/039502.
- Langenbrunner, B., and J. Neelin (2013), Analyzing ENSO teleconnections in CMIP models as a measure of model fidelity in simulating precipitation, *J. Clim.*, doi:10.1175/JCLI-D-12-00542.1, in press.
- Mantua, N. J., S. R. Hare, Y. Zhang, J. M. Wallace, and R. C. Francis (1997), A Pacific interdecadal climate oscillation with impacts on salmon production, *Bull. Am. Meteorol. Soc.*, *78*, 1069–1079, doi:10.1175/1520-0477(1997)078<1069:APICOW>2.0.CO;2.
- McCabe, G. J., and M. D. Dettinger (1999), Decadal variations in the strength of ENSO teleconnection with precipitation in the Western United States, *Int. J. Climatol.*, *19*, 1399–1410.
- Meehl, G. A., G. J. Boer, C. Covey, M. Latif, and R. J. Stouffer (2000), The coupled model intercomparison project (CMIP), *Bull. Am. Meteorol. Soc.*, *81*, 313–318.
- Mo, K.C., J.-K. Schemm, H. M. H. Juang, R. W. Higgins, and Y. Song (2005), Impact of model resolution on the prediction of summer precipitation over the United States and Mexico, *J. Clim.*, *18*, 3910–3927, doi:10.1175/JCLI3513.1.
- Rotstayn, L. D., M. A. Collier, M. R. Dix, Y. Feng, H. B. Gordon, S. P. O'Farrell, I. N. Smith, et al. (2010), Improved simulation of Australian climate and ENSO-related rainfall variability in a global climate model with an interactive aerosol treatment, *Int. J. Climatol.*, *30*(7), 1067–1088, doi:10.1002/joc.1952.
- Schneider, N., and B. D. Cornuelle (2005), The forcing of the Pacific Decadal Oscillation, *J. Clim.*, *18*, 4355–4373.

- Schneider, U., A. Becker, A. Meyer-Christoffer, M. Ziese, and B. Rudolf (2011), Global precipitation analysis products of the GPCP. [Available at ftp://ftp-anon.dwd.de/pub/data/gpcp/PDF/GPCP_intro_products_2008.pdf.]
- Smith, T. M., R. W. Reynolds, T. C. Peterson, and J. Lawrimore (2008), Improvements to NOAA's historical merged land-ocean surface temperature analysis (1880–2006), *J. Clim.*, *21*, 2283–2296.
- Swetnam, T. W., and J. L. Betancourt (1998), Mesoscale disturbance and ecological response to decadal climatic variability in the American southwest, *J. Clim.*, *11*, 3128–3147.
- Taylor, K. E., R. J. Stouffer, and G. A. Meehl (2012), An Overview of CMIP5 and the experiment design, *Bull. Am. Meteorol. Soc.*, *93*(4), 485–498, doi:10.1175/BAMS-D-11-00094.1.
- Westerling, A., and T. Swetnam (2003), Interannual to decadal drought and wildfire in the western United States, *EOS*, *84*, 545–560.
- Zhang, Y., Y. Qian, V. Duliere, E. Salathe, and L. Leung (2012), ENSO anomalies over the Western United States: present and future patterns in regional climate simulations, *Clim. Change*, *110*, 315–346.